Journal of Chromatography, 638 (1993) 155–164
Elsevier Science Publishers B.V., Amsterdam

CHROM. 24 941

Computer simulation and experimental validation of the electrophoretic behavior of proteins

III. Use of titration data predicted by the protein's amino acid composition

Richard A. Mosher

Center for Separation Science, University of Arizona, Tucson, AZ 85721 (USA)

Petr Gebauer[☆] and Wolfgang Thormann[*]

Department of Clinical Pharmacology, University of Berne, Murtenstrasse 35, CH-3010 Berne (Switzerland)

ABSTRACT

To simulate the electrophoretic behavior of a protein, a diffusion coefficient and a tabular representation of net charge *vs.* pH (titration curve) are required. So far data taken from the literature have been employed, the tables being extracted from experimentally determined titration curves. The construction of data tables from the amino acid composition of proteins is reported and compared with those from the literature. The predicted data serve as a rough approximation only, because pK values are dependent on the local environment. Shifting the curve along the pH axis to match the experimentally determined pI is shown to yield simulation data which is in better agreement with experimental data. However, the predicted protein charge numbers are typically too large. Reduction by a pH-independent factor is shown to provide meaningful data for computer simulation. The utility of the titration data employed is documented with good agreement between simulation and experimental data obtained by capillary isotachophoresis.

INTRODUCTION

Computer simulation of electrophoresis has become an important research tool. Qualitative and quantitative agreement of simulation data with experimental results have confirmed the utility of simulations for the prediction of separability, separation dynamics, zone characteristics and boundary structure, and for the reproduction and explanation of some experimentally observed phenomena [1]. Most of the simulation work performed so far has been limited to low-molecular-mass compounds. Few computer models are available that treat proteins. The complexity inherent in dealing with these macromolecules arises primarily from the lack of a straightforward mathematical procedure for dealing with their ionization [2–4]. The simulation model used in this work has been described in detail previously [2,4]. It is one-dimensional, based on the principles of electroneutrality and conservation of mass and charge and assumes isothermal conditions. Relationships between the concentrations of the

* Corresponding author.
☆ Permanent address: Institute of Analytical Chemistry, Czech Academy of Sciences, CS-611 42 Brno, Czech Republic.

0021-9673/93/$06.00

various species of a low-molecular-mass component are described by equilibrium constants. The large number of dissociating groups on a protein generates a population of molecules that possess an average net charge at any given pH. The mean square charge of this population is used to describe the contribution of the protein to the current density. In order to make the protein mobility a function of ionic strength, the Linderstrøm–Lang approach is employed [4].

To simulate the behavior of a protein and to calculate its net mobility, two inputs are required, a diffusion coefficient (serving for calculation of the protein radius and diffusive mass transport) and a tabular representation of net charge *vs.* pH (titration curve). So far data taken from the literature have been employed, the table being extracted from experimentally determined titration curves [1,2,4,5]. It is important to note that such titration data are dependent on the ionic strength and are measured at one or more fixed ionic strengths. Titration data that have been extrapolated to zero ionic strength were used when available. Data taken at low ionic strength have generally been found to yield simulation data that are in good agreement with experimental data obtained in media of low ionic strength, such as those employed in isotachophoresis (ITP) [4].

Protein titration curves [6], and also electrophoretic mobilities [7] and p*I* values [8], can be predicted from the protein's amino acid content by applying a model based on the Henderson–Hasselbalch equation. This approach assumes that any specific ionizing group has the same p*K* everywhere on the molecule. For two proteins with known, experimentally determined p*K* values of the residues, calculated input tables have been shown to be in good agreement with experimental titration data [1]. However, the availability of either experimental titration data or accurate p*K* values for the residues within a protein is limited to a small number of proteins. Therefore, titration data generated using the amino acid composition of a protein and p*K* values of free amino acids have been evaluated for use in the simulation of protein electrophoretic behavior.

THEORETICAL CONSIDERATIONS

For simplicity, it is assumed that each specific ionizing group of a protein has the same p*K* everywhere on the molecule. Hence the net charge of a protein molecule is given by

$$\text{net charge} = \sum_i \frac{n_i}{\frac{K_i}{[H^+]} + 1} - \sum_j \frac{n_j}{\frac{[H^+]}{K_j} + 1} + z_L \quad (1)$$

where n_i and K_i denote the number and ionization constant, respectively, of a weakly basic group i, n_j and K_j the corresponding values of a weakly acidic group j and z_L represents the total charge of ligands bound to the protein. Typically there are four different basic groups ($i = 4$), which includes the α-amino group, the imidazole group of histidine, the ε-amino group of lysine and the guanidinium group of arginine. The common weakly acidic groups comprise the α-carboxyl group, the β- and γ-carboxyl groups of aspartic and glutamic acid, respectively, the phenolic group of tyrosine and the thiol of cysteine, yielding a value of 5 for j. There are n of each group present and it is assumed that the

TABLE I

RESIDUE-SPECIFIC p*K* VALUES USED IN THIS WORK

Residue	Tanford and Hauenstein [10]	Compton [7]	GCG [11]
Basic			
Arg	12.00	12.00	12.50
Lys	10.10	10.40	10.79
His	6.50	6.40	6.50
t-NH_2	7.80	8.20	8.56
Acidic			
Glu	4.60	4.50	4.25
Asp	4.60	4.00	3.91
Cys	–	9.00	8.30
Tyr	9.60	10.00	10.95
t-COOH	3.75	3.20	3.56

TABLE II

AMINO ACID COMPOSITION OF PROTEINS USED IN THIS WORK

Amino acid composition according to GCG [11].

Amino acid	RNase	BLB	OVA	CYTC
Arg	4	3	15	2
Lys	10	15	20	19
His	4	2	7	3
t-NH_2	1	1	1	1
Glu	5	16	33	9
Asp	5	10	14	3
Cys	8	5	6	2
Tyr	6	4	10	4
t-COOH	1	1	1	1

dissociation constants (K) are equal for all members of a group. Charged ligands bound to the protein are typically metal ions, such as Fe^{2+} in hemoglobin for which z_L equals 8 or Fe^{3+} in cytochrome c (CYTC) with $z_L = 3$. A variety of values for the pKs of free amino acids, and the N (t-NH_2) and C (t-COOH) termini of proteins, can be found in the literature [9]. Three sets of these values have been compared in this work (Table I). One of these is based on experimental values for a specific protein [10], one from the recent literature [7] and one from the Genetics Computer Group (GCG) database of protein amino acid composition [11] (Table II).

EXPERIMENTAL

Chemicals

The chemicals used were of analytical-reagent or research grade. Ribonuclease A (RNase) from bovine pancreas and CYTC from horse heart were obtained from Sigma (St. Louis, MO, USA), ovalbumin (OVA) from chicken egg from Serva (Heidelberg, Germany) and β-lactoglobulin B (BLB) from bovine milk from Koch-Light (Haverhill, UK).

Computer simulations

The extended and PC-adapted model of Mosher *et al.* [4] was used. A Mandax AT 286 12 MHz computer (Panatronic, Zürich, Switzerland) running at 12 MHz and featuring a mathematical coprocessor or an Excel AT 486 computer (Walz Computer, Berne, Switzerland) running at 50 MHz were employed throughout this work. Initial conditions that must be specified for a simulation include the distribution of all components, the diffusion coefficients and net charge–pH relationships of the proteins, the pK and mobility values of the buffer constituents, the current density and the duration of the current flow. The program outputs concentration, pH and conductivity profiles as functions of time. The input data for low-molecular-mass components are summarized in Table III. The net charge–pH relationships for the proteins were calculated using eqn. 1 together with the pK values and amino acid compositions listed in Tables I and II, respectively. The experimental net charge–pH relationships and diffusion coefficients for the proteins were taken from literature data [12–19].

Experimental validation by capillary ITP

The experiments were performed on a Tachophor 2127 isotachophoretic capillary analyzer (LKB, Bromma, Sweden) equipped with a

TABLE III

ELECTROCHEMICAL PARAMETERS OF SMALL MOLECULES USED IN SIMULATION

Compound[a]	pK_1	pK_2	Mobility ($m^2/V \cdot s \times 10^9$)
Acetic acid	4.76		42.4
K^+			79.1
TPA			18.1
GABA	4.23	10.43	32.0
H^+			362.7
OH^-			198.7

[a] TPA = Tetrapentylammonium; GABA = γ-aminobutyric acid.

28 cm × 0.5 mm I.D. PTFE capillary and a conductivity and UV detector (iodine lamp and 277-nm filter) at the column end. Zone patterns were recorded on a two-pen strip-chart recorder as they migrated across the points of detection. The cationic electrolyte systems used consisted of 0.01 *M* potassium acetate and acetic acid (pH_L 4.75) as the leader and 0.01 *M* acetic acid as the terminator. Unless stated otherwise, all measurements were performed at a constant current of 150 μA (the initial and final voltages were about 2.5 and 8.5 kV, respectively) provided by the Tachophor 2127 power supply (500 μA maximum; 30 kV maximum). Samples (1–4 μl containing mg/ml and m*M* concentrations of proteins and spacers, respectively) were injected with a 10-μl syringe (Hamilton, Bonaduz, Switzerland).

RESULTS AND DISCUSSION

The titration curves for four proteins, bovine pancreas RNase, horse heart CYTC, bovine milk BLB and hen egg OVA, whose amino acid compositions are given in Table II, were determined using eqn. 1. Plots for one protein, RNase, calculated using the three different sets of p*K* values listed in Table I, are presented in Fig. 1A. The data of Compton [7] and Tanford and Hauenstein [10] are in close agreement when cysteine (Cys) with a p*K* of 9 is incorporated for both curves. Larger differences are seen with the p*K*s of GCG. All three calculated graphs deviate from the experimental titration curve [10] (broken line), with the deviation being most pronounced in the pH range above 8, *i.e.*, around the isoelectric point. Calculated p*I* values of the four proteins of interest, using each of the three sets of p*K* values, are given in Table IV. Table IV also includes experimental data, together with p*I* values calculated without including Cys, as was originally suggested for RNase by Tanford and Hauenstein [10]. For BLB and OVA, omitting Cys has no impact on the p*I*, whereas for RNase and CYTC lower p*I* values are predicted with inclusion of Cys. Eqn. 1 also permits the consideration of charges contributed by tightly bound molecules or ions which are not part of the protein's primary

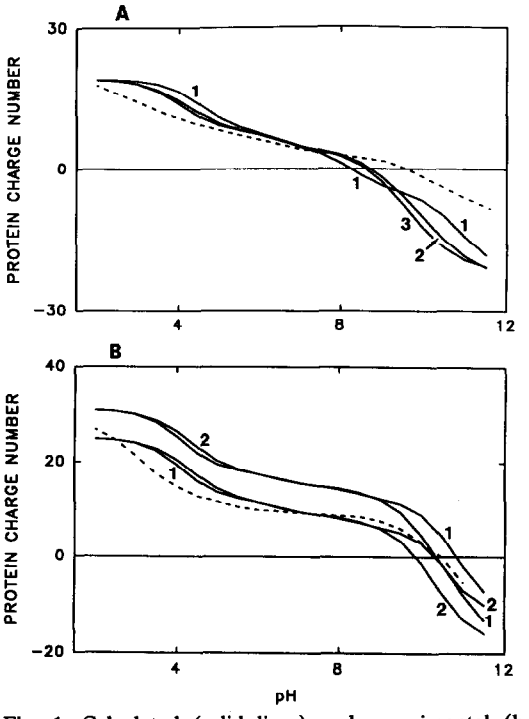

Fig. 1. Calculated (solid lines) and experimental (broken lines) titration data for (A) RNase and (B) CYTC. The curves obtained with the amino acid p*K*s of GCG [11], Compton [7] and Tanford and Hauenstein [10] are denoted 1, 2 and 3, respectively. Upper and lower graphs in (B) refer to a ligand charge of 3 and 0, respectively.

TABLE IV

CALCULATED AND EXPERIMENTAL p*I* VALUES

Amino acid composition according to GCG [11] and p*I* determination extracted from the titration curve calculated by eqn. 1 and using the p*K* values of Tanford and Hauenstein [10], Compton [7] and GCG [11], respectively (Table I).

Parameter	Protein				
	RNase (0)[a]	BLB (0)[a]	OVA (0)[a]	CYTC	
				0[a]	3[a]
p*I* [10][b]	9.20	5.15	5.48	9.71	10.23
p*I* [10][c]	8.59	5.15	5.48	9.58	10.07
p*I* [7]	8.69	4.89	5.31	9.87	10.37
p*I* [11]	8.23	4.70	5.10	10.34	10.85
p*I* (exp.)	9.60 [10]	5.18 [13]	4.90 [16]	10.49 [18]	

[a] Ligand charge.
[b] No Cys considered.
[c] With inclusion of Cys using a p*K* of 9.

structure. As an example, titration data for CYTC with and without inclusion of the three positive charges of the Fe^{3+} ion were calculated. As is shown in Table IV and Fig. 1B, incorporation of the three charges produces a p*I* shift of about +0.5 pH unit (Table IV) and increased protein charge numbers (Fig. 1B). Unexpectedly, disregarding the contribution of Fe^{3+} produced a better agreement between calculated and experimental (broken line in Fig. 1B) titration curves.

Table V gives the titration data obtained with the GCG input data which were employed for the simulations performed. Table VI presents the different input conditions and predicted ITP zone characteristics of cationically migrating BLB, RNase, CYTC and OVA using 10 m*M* potassium acetate adjusted with acetic acid to pH 4.75 as leader and acetic acid as terminator. The model predicted the formation of an ITP zone with a characteristic plateau concentration and distinct protein mobility for each case. The protein zone properties, however, are clearly dependent on the titration curve employed. For each protein, the first line of data was obtained with the calculated titration curve listed in Table V, whereas the characteristics predicted with the use of experimental titration data are listed in the last line. Additionally, Table VI presents cationic protein ITP data obtained with calculated titration data which were modified by a specified pH shift and/or a factor which reduced the calculated charge number. The data are discussed in turn. The goal is a calculated titration curve that closely reproduces the simulation behavior obtained with an experimental titration curve.

TABLE V

PROTEIN INPUT DATA

Data calculated using the GCG data in Tables I and II.

pH	RNase	CYTC	BLB	OVA
2.0	18.88	24.89	20.76	42.62
2.5	18.64	24.65	20.27	41.82
3.0	17.97	23.98	18.84	39.49
3.5	16.38	22.33	15.32	33.62
4.0	13.70	19.36	8.98	22.64
4.5	10.88	15.93	1.89	9.77
5.0	9.04	13.53	−2.86	0.85
5.5	8.03	12.29	−5.08	−3.53
6.0	7.13	11.45	−6.14	−6.02
6.5	5.91	10.52	−6.97	−8.38
7.0	4.56	9.61	−7.75	−10.57
7.5	3.19	8.91	−8.58	−12.26
8.0	1.21	8.17	−9.85	−14.04
8.5	−1.40	7.23	−11.60	−16.21
9.0	−3.62	6.26	−13.18	−18.15
9.5	−5.12	5.16	−14.47	−19.87
10.0	−6.82	3.01	−16.37	−22.69
10.5	−9.94	−1.48	−20.12	−28.50
11.0	−14.46	−7.92	−25.47	−37.10

Fig. 2 presents the simulated ITP steady-state distributions of a two-protein system (RNase and CYTC) using (A) the experimental input data and (B) the calculated titration data. Protein concentrations (upper graphs) and conductivity and pH profiles (lower graphs) are shown for 150 min of current flow. In both instances RNase and CYTC are predicted to behave as typical ITP samples, forming a stack of continuous plateau-shaped zones between the leader (L) and terminator (T) with CYTC appearing immediately behind the leader. This predicted order and the characteristic, step-like conductivity changes have been confirmed experimentally (Fig. 2C). The experimental data represent the UV absorption (277 nm) and conductivity (expressed as increasing resistance *R*) capillary ITP data measured with the Tachophor. Owing to the serial mounting of the two detectors at the capillary end, there is a small shift of detection time, the UV absorbance response being recorded before the conductivity. Although the current densities employed differ by more than two orders of magnitude (experiment, *ca.* 765 A/m^2; simulation, 10 A/m^2) there is similarity between predicted and experimental protein zone shapes and conductivity distributions. These data demonstrate that calculated, unmodified titration curves can sometimes be used to predict relative net mobilities of two proteins in a given ITP buffer system.

Fig. 3A indicates that calculated titration curves are not always effective predictors of experimental behavior. The computer-predicted dynamics of the separation of RNase, BLB and OVA using the calculated titration data (Table

TABLE VI

INPUT AND SIMULATION RESULTS FOR CATIONIC ITP OF DIFFERENT PROTEINS

Titration data were calculated with eqn. 1 using amino acid composition and pK values according to GCG (Tables I and II). All simulations were performed with the model incorporating the Linderstrøm–Lang approximation (for details see ref. 4). Diffusion coefficients for proteins employed were BLB 7.48 [14], RNase 13.6 [15], CYCT 13.3 [19] and OVA $7.76 \cdot 10^{-11}$ m^2/s [17].

Line No.	Protein	Titration curve modification		pI	Protein concentration (mM)	Acetate concentration (mM)	Conductivity ($S/m \times 10^2$)	pH	Net mobility ($m^2/V \cdot s \times 10^9$)	
		Shift	Factor						Protein	Acetate
1	RNase	–	–	8.23	0.639	17.04	5.12	4.58	34.3	16.8
2	RNase	0.7	–	8.93	0.553	17.96	6.65	4.64	44.6	18.4
3	RNase	1.4	–	9.63	0.495	18.62	8.00	4.69	53.7	19.4
4	RNase	1.4	0.603	9.63	0.641	17.02	5.14	4.58	34.4	16.9
5	RNase	0.7	0.603	8.93	0.691	16.51	4.38	4.53	29.4	15.8
6	RNase	–	0.603	8.23	0.768	15.80	3.42	4.45	23.0	13.9
7	RNase	Tanford and Hauenstein [10]		9.60	0.686	16.56	4.47	4.54	30.0	16.0
8	CYTC[a]	–	–	10.34	0.526	18.08	6.88	4.65	46.2	18.6
9	CYTC[a]	–	0.603	10.34	0.660	16.61	4.52	4.54	30.3	16.0
10	CYTC	Theorell and Akesson [18]		10.49	0.583	17.43	5.77	4.61	38.7	17.7
11	BLB	–	–	4.70	0.387	15.33	1.80	4.12	12.1	7.9
12	BLB	0.5	–	5.20	0.368	15.19	2.60	4.34	17.4	11.7
13	BLB	0.5	0.603	5.20	0.394	14.99	1.94	4.19	13.0	9.0
14	BLB	–	0.603	4.70	0.366	16.15	1.52	3.96	10.2	5.8
15	BLB	Cannan *et al.* [13]		5.18	0.368	15.19	2.58	4.34	17.4	11.6
16	OVA	–	–	5.10	0.364	15.63	3.00	4.38	20.1	12.6
17	OVA	−0.5	–	4.60	0.407	15.32	1.83	4.13	12.3	8.04
18	OVA	−0.2	–	4.90	0.390	15.27	2.44	4.30	16.3	10.9
19	OVA	−0.5	0.603	4.60	0.391	15.94	1.60	4.00	10.7	6.33
20	OVA	−0.2	0.603	4.90	0.406	15.22	1.97	4.18	13.2	8.85
21	OVA	–	0.603	5.10	0.396	15.19	2.32	4.27	15.6	10.4
22	OVA	−0.2	0.244	4.90	0.352	16.96	1.45	3.87	9.72	4.81
23	OVA	Cannan *et al.* [16], $I \rightarrow 0$		4.90	0.406	15.52	1.65	4.06	11.0	7.01

[a] No ligand charge considered.

V) for each protein are presented. Again, all proteins are predicted to behave as typical ITP samples, forming a stack of contiguous plateau-shaped zones between the leader and terminator with RNase (zone 1) appearing immediately behind the leader, followed by OVA (zone 5) and BLB (zone 3). This predicted order is not consistent with that obtained using the experimental titration curves (Fig. 3D), which predict BLB located between RNase and OVA.

The measured isotachopherogram (Fig. 4A) agrees with the simulation data obtained with the experimental input data. This is also reflected in the net mobilities predicted using the calculated titration curves (lines 11 and 16 in Table VI) which are inverted with respect to those predicted employing the experimental titration data (lines 15 and 23). These results reveal the limited utility of calculated titration curves for the simulation of ITP behavior. The discrepancy in the pI values with respect to experimental data is one obvious shortcoming of this approach. The effect of simply shifting the calculated titration curves along the pH axis to the experimental pI values

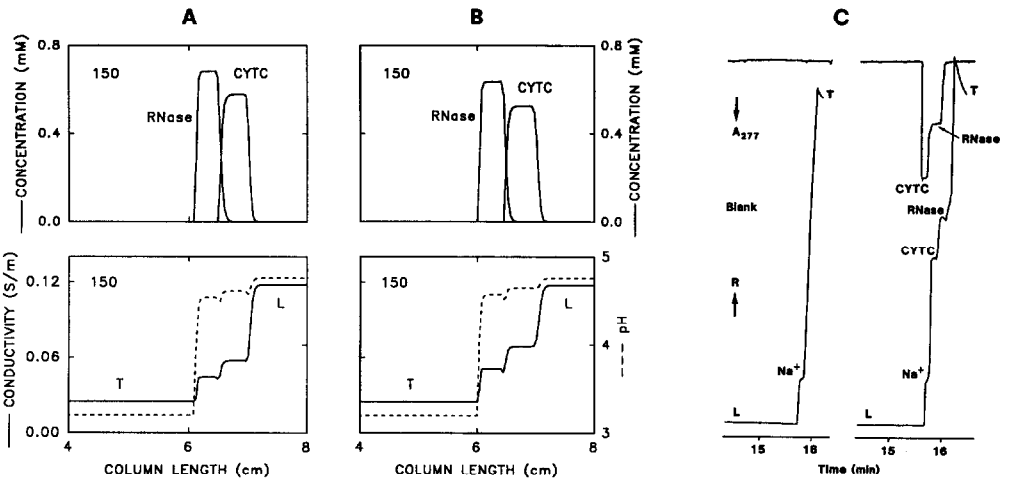

Fig. 2. Cationic ITP of RNase and CYTC. (A) and (B) show the predicted steady-state concentration distributions (upper half) and pH and conductivity profiles (broken and solid lines, respectively, in lower half) after 150 min of current flow (10 A/m^2) using experimental and calculated (corresponding to lines 1 and 8 in Table VI) protein input data, respectively. (C) Experimental Tachophor records of blank (left isotachopherogram) and the detected ITP stack with CYTC and RNase as sample (right isotachopherogram). Both the steady-state absorbance at 277 nm (upper graphs) and conductivity profile expressed as increasing resistance *R* (lower graphs) are presented. For the simulation the initial sample pulses (between 0.6 and 1 cm) contained CYTC and RNase (0.7 m*M* each). In the experiment, Na^+ represents an impurity and L and T refer to leader and terminator, respectively.

was therefore evaluated. pH shifts of 1.4, 0.5 and −0.2 units for RNase, BLB and OVA, respectively, were implemented (lines 3, 12 and 18 in Table VI). Simulation of the separation of the three proteins using these modified input data predicted the proper migration sequence in this buffer system (compare Fig. 3B and D). There were, however, significant differences in the zone properties, as is reflected in the corresponding data in Table VI.

The shift of 1.4 pH units for RNase produced predicted zone properties (*e.g.*, protein concentration and net mobility) that corresponded to those with experimental titration data less well than did those with the unshifted curve. This is due to the increased charge number of the molecule at the system pH and is reflected in the increased net mobility. The predicted zone properties of OVA with pH shift improved with respect to those obtained with the experimental titration curve. The shift decreased the charge number on the protein. For BLB, the pH shift brought the predicted zone properties into excellent agreement with those produced by the experimental titration data. These data are consistent with two conclusions. The first is that the titration curve used for simulation must reflect the experimental p*I*. This is of obvious importance for the simulation of the isoelectric focusing behavior of proteins and clearly also for simulating ITP and zone electrophoretic behavior. The second conclusion is that calculated titration curves with accurate p*I*s generally, although not always, overestimate the charge on a molecule. The calculated, unshifted titration curve of RNase produced zone properties that were serendipitously close to those produced by the experimental curve. When shifted to the experimental p*I*, the molecule displayed a substantially increased charge at the system pH. The net mobility in this buffer system is much higher with the calculated, shifted curve than with the experimental curve (lines 3 and 7 in Table VI). This is true for OVA (lines 18 and 23) and for CYTC (lines 8 and 10). The titration curve was not shifted for this last example, but the conclusion is valid. The shift would move the p*I* away from the system pH, thus increasing the net charge on the molecule and its net mobility in the buffer system (compare lines 1–3 and 11 with

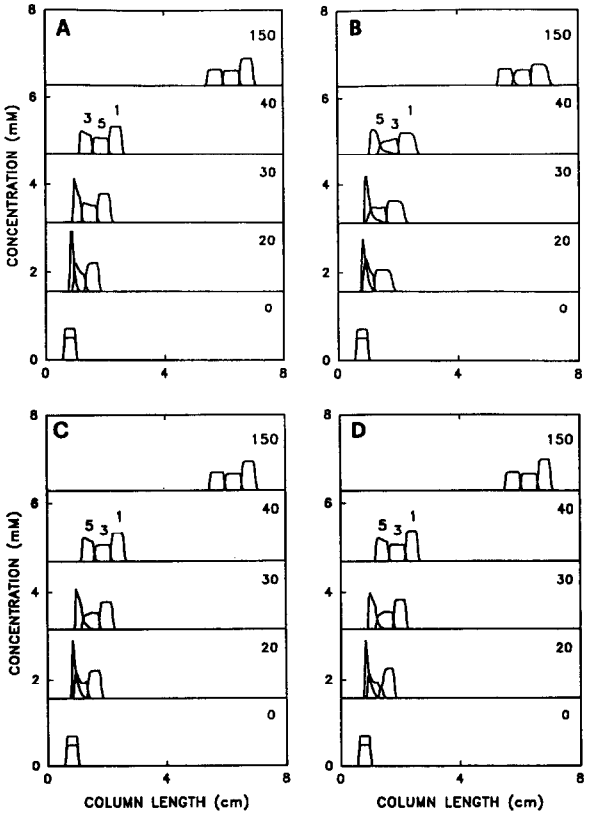

Fig. 3. Computer-simulated separation dynamics of OVA (5), BLB (3) and RNase (1) using (A) calculated titration data, (B) calculated titration data shifted −0.2, 0.5 and 1.4 pH units for the three proteins, respectively, (C) titration data as in (B) with the charge numbers of OVA and RNase being multiplied by 0.603 and (D) experimental titration data. For the simulation, the initial conditions included pulses of OVA, BLB and RNase at 0.5, 0.5 and 0.7 m*M*, respectively, located between 0.6 and 1 cm of the column length. The current density was 10 A/m^2. All panels show the concentration profiles of the three proteins at the indicated time intervals between 0 and 150 min.

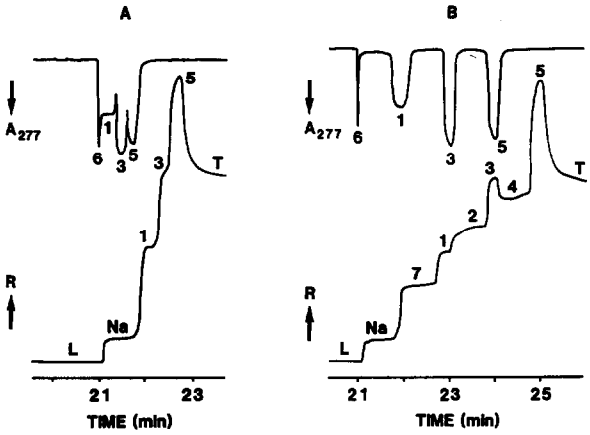

Fig. 4. Experimental ITP data (adapted from ref. 4) showing the steady-state distribution of (A) RNase (1), BLB (3) and OVA (5) and (B) the same protein mixture spaced with TPA (2) and GABA (4). Absorbance at 277 nm (upper graphs) and conductivity profiles expressed as increasing resistance *R* (lower graphs) are presented. While recording the experimental data, the current was reduced to 50 μA. Zone 6 and Na represent impurities and zone 7 represents tris-(hydroxymethyl)aminomethane, which was used to isolate the impurities from the proteins. L and T refer to leader and terminator, respectively.

12). Correspondingly, a shift that would move the p*I* towards the system pH would result in a decrease in net charge and mobility (compare lines 16–18).

There is a clear requirement to reduce the charge numbers calculated for proteins. This need arises from the role of electrostatic charge suppression in decreasing the apparent valence of proteins [20]. As it has been shown that the electrophoretic mobility of a protein is directly proportional to charge number over the entire pH range [7], a pH-independent factor can be employed. Longsworth [12] used 0.603 to approach a similar problem with OVA and his value was arbitrarily chosen as a starting point. The data in Table VI show that reducing the protein valence by this factor yields predicted zone characteristics for RNase (line 4) which are in better agreement with those produced using the experimental titration curve than are the zone characteristics produced with the shifted curve. A clear improvement is also obtained with OVA. As the predicted data for BLB were already in good agreement after the pH shift, reducing the valence resulted in zone characteristics that agreed less well with the data produced using the experimental curve. Corresponding simulated protein zone distributions of the separation of RNase, BLB and OVA (Fig. 3C) are shown to agree well with those obtained with the experimental input data (Fig. 3D). It is important to note that valence reduction without pH shift (lines 6, 9, 14 and 21 in Table VI) did not provide accurate data for the four proteins.

An important aspect of protein separation by

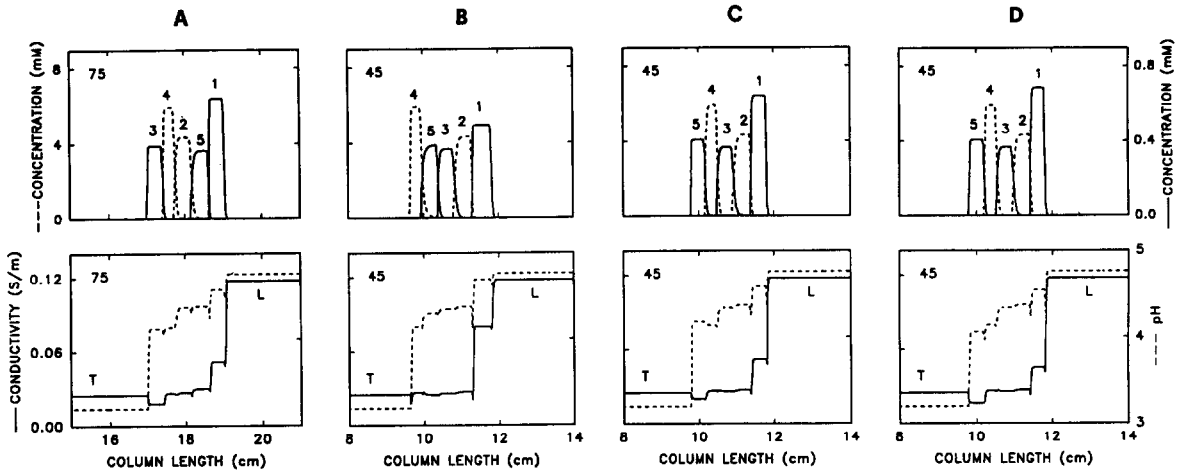

Fig. 5. Computer prediction of the ITP separation of RNase (zone 1), TPA (2), BLB (3), GABA (4) and OVA (5) using (A) calculated titration data, (B) calculated protein titration data shifted 1.4, 0.5 and −0.2 pH units for the three proteins, respectively, (C) titration data as in (B) with the charge numbers of OVA and RNase being multiplied by 0.603 and (D) experimental titration data. The initial sample pulse (between 0.64 and 0.96 cm) consisted of 0.5 m*M* OVA, 0.5 m*M* BLB, 0.8 m*M* RNase, 6 m*M* TPA and 6 m*M* GABA. The current density was 60 A/m^2. All panels show the concentration profiles (upper graphs) and the conductivity and pH distributions (solid and broken lines, respectively, lower graphs) at the indicated time intervals.

ITP involves the use of low-molecular-mass molecules as spacers to achieve the fractionation of complex mixtures into several sub-mixtures or to separate completely two proteins that would otherwise migrate contiguously. The simulated behavior of a system composed of the same three proteins (RNase, BLB and OVA) and two low-molecular-mass spacers [tetrapentylammonium (TPA) and γ-aminobutyric acid (GABA)] is presented in Fig. 5. The predicted zone properties of the low-molecular-mass compounds are given in Table VII. The predicted migration order with the use of the experimental protein input data is RNase, TPA, BLB, GABA and OVA (Fig. 5D). Hence the spacers are predicted to separate the three proteins. This migration order has been confirmed experimentally (Fig. 4B). Performing the same simulation with calculated protein titration data produced a different behavior (Fig. 5A), with the prediction of a completely different steady-state zone sequence. Shifting of the protein input data along the pH

TABLE VII

SIMULATED ITP ZONE PROPERTIES OF LOW-MOLECULAR-MASS COMPOUNDS

Parameter	Zone			
	Leader (K^+)	Samples		Terminator (H^+)
		TPA	GABA	
Concentration (m*M*)	10	4.34	5.93	0.0634
Acetate concentration (m*M*)	20	15.11	17.34	23.75
pH	4.76	4.37	4.14	3.20
Conductivity (S/m × 10^2)	11.79	2.70	2.63	2.48
Mobility ($m^2/V \cdot s \times 10^9$)	79.10	18.10	17.67	16.62
Acetate mobility ($m^2/V \cdot s \times 10^9$)	21.24	12.29	8.18	1.13

axis to the correct isoelectric point resulted in the steady-state pattern shown in Fig. 5B, in which zones 4 and 5 are in reverse order compared with the experimentally confirmed pattern in Fig. 5D. Reduction of the charge numbers of RNase and OVA with the pH-independent factor of 0.603 (see above) provided the correct zone pattern (Fig. 5C), which is in good agreement with that obtained with the experimental protein titration data (Fig. 5D).

The good agreement between the data in Fig. 5C and D indicated that protein titration curves useful for the simulation of electrophoretic behavior can be generated employing the GCG database of amino acid composition and pK values and eqn. 1 to generate a titration curve. This curve must then be shifted along the pH axis to match the experimental pI, and the calculated charge numbers reduced throughout the pH range by 0.603. The limitation of this approach is shown by BLB, which required no reduction in charge number to reflect the experimental data. The selection of a charge reduction factor is at present an arbitrary process. Compton and O'Grady [6] attempted to predict such factors. Their suggested value of 0.244 for OVA was found to be too small to allow accurate simulation of ITP behavior (lines 22 and 23 in Table VI). Much more work is needed on this subject.

ACKNOWLEDGEMENTS

The authors are grateful to Dr. M. Solioz for providing access to the GCG database. This work was supported by the Swiss National Science Foundation.

REFERENCES

1 R.A. Mosher, D.A. Saville and W. Thormann, *The Dynamics of Electrophoresis*, VCH, Weinheim, 1992.
2 R.A. Mosher, D. Dewey, W. Thormann, D.A. Saville and M. Bier, *Anal. Chem.*, 61 (1989) 362.
3 G.O. Roberts, P.H. Rhodes and R.S. Snyder, *J. Chromatogr.*, 480 (1989) 35.
4 R.A. Mosher, P. Gebauer, J. Caslavska and W. Thormann, *Anal. Chem.*, 64 (1992) 2991.
5 W. Thormann and R.A. Mosher, *Electrophoresis*, 11 (1990) 292.
6 B.J. Compton and E.A. O'Grady, *Anal. Chem.*, 63 (1991) 2597.
7 B.J. Compton, *J. Chromatogr.*, 539 (1991) 357.
8 A. Sillero and J.M. Ribeiro, *Anal. Biochem.*, 179 (1989) 319.
9 V. Kašička and Z. Prusík, *J. Chromatogr.*, 569 (1991) 123.
10 C. Tanford and J.D. Hauenstein, *J. Am. Chem. Soc.*, 78 (1956) 5287.
11 J. Devereux, P. Haeberly and O. Smithies, *Nucleic Acids Res.*, 12 (1984) 387.
12 L.G. Longsworth, *Ann. N.Y. Acad. Sci.*, 41 (1941) 267.
13 R.K. Cannan, A.H. Palmer and A.C. Kibrick, *J. Biol. Chem.*, 142 (1942) 803.
14 A.L. Lehninger, *Biochemistry*, Worth, New York, 2nd ed., 1975, p. 176.
15 D.M. Greenberg, *Amino Acids and Proteins*, Charles C. Thomas, Springfield, IL, 1951, p. 394.
16 R.K. Cannan, A.C. Kibrick and A.H. Palmer, *Ann. N.Y. Acad. Sci.*, 41 (1941) 243.
17 A. Tiselius and H. Svensson, *Trans. Faraday Soc.*, 36 (1940) 16.
18 H. Theorell and A. Akesson, *J. Am. Chem. Soc.*, 63 (1941) 1818.
19 J.T. Adsall, in H. Nerath and K. Baile (Editors), *The Proteins, Chemistry, Biological Activity and Methods*, Vol. 1, Part B, Academic Press, New York, 1953, p. 634.
20 C. Tanford and J.G. Kirkwood, *J. Am. Chem. Soc.*, 79 (1957) 5333.